Spin and charge fluctuations in α-structure layered nitride superconductors

Quan Yin,[*] Erik R. Ylvisaker, and Warren E. Pickett

Department of Physics, University of California, Davis, California 95616, USA
(Received 5 November 2010; published 19 January 2011)

To explore conditions underlying the superconductivity in electron-doped TiNCl where $T_c = 16$ K, we calculate the electronic structure, Wannier functions, and spin and charge susceptibilities using first-principles density functional theory. TiNCl is the first high-temperature superconductor discovered in the α structure of the layered transition-metal nitride family MNCl (M = Ti,Zr,Hf). We construct a tight-binding model based on Wannier functions derived from the band structure, and consider explicit electronic interactions in a multiband Hubbard Hamiltonian, where the interactions are treated within the random phase approximation to calculate spin and charge susceptibility. The results show that, consistent with TiNCl being a nonmagnetic material, spin fluctuations do not dominate over charge fluctuations and both may have comparable impact on the properties of the doped system.

I. INTRODUCTION AND BACKGROUND

High-temperature superconductivity (HTSC) has been a widely pursued subject for condensed matter physicists for over two decades. There are several classes of materials where unconventional superconductivity is found: cuprates whose highest T_c's remain unrivaled, the recently discovered and intensively studied iron pnictides, $Na_{1-x}CoO_2$ intercalated with H_2O, $BaBiO_3$ doped by K, the Pu-based "115" heavy-fermion series, and the transition-metal nitride halides MNX (M = Zr,Hf; X = Cl,Br,I). MNX crystallizes in two structures, labeled α and β. The Zr and Hf members were found to be superconducting with unprecedented critical temperatures for nitrides (15 K, 25 K) in the β structure, which is isostructural to SmSI, and contains double-honeycomb layers of alternating M and N atoms.[1] The sister compound TiNCl with α structure has now been discovered to superconduct (16 K) as well.[2]

Based on many examples now, layered structures seem to favor high-temperature superconductivity. The reduced dimensionality promotes various instabilities associated with Fermi surface nesting. Due to electron-electron interactions, many parent compounds of HTSCs exhibit long-range magnetic order, such as antiferromagnetism (AFM) in cuprates and iron pnictides. The AFM order needs to be destroyed upon doping, by electrons or by holes, to open the way for superconductivity. This is not the case for nonmagnetic MNX, which are band insulators with a band gap of 2–4 eV, and the transition-metal d states make up most of the lower conduction bands.[3]

Both the α and β polymorphs are quasi-two-dimensional (quasi-2D) structures with large interlayer spacing and weak van der Waals coupling between layers. When doped with electrons, A_xMNX (A being alkali metals) remains insulating at low concentration, then suddenly become superconducting at about $x = 0.13$ in HfNCl and $x = 0.06$ in ZrNCl, and maintains a relatively constant T_c up to $x = 0.5$ (Ref. 4). The superconducting transition temperature can be as high as 26 K, discovered in $Li_x(THF)_yHfNCl$.[5] It has also been found that T_c may be correlated with the interlayer spacing, which can be tuned by intercalation of different-sized molecules.[6] Also, the electron doping can be substituted by ion vacancy of the Cl atoms with similar superconductivity being found.[7] In a theoretical treatment by Bill *et al.*, the dynamical screening of electronic interactions in these materials was modeled[8,9]

by conducting sheets spaced by dielectrics.[10] A fully open large superconducting gap without nodes was observed with tunneling spectroscopy.[11–13]

Experimental observations from several perspectives confirm that MNX are not electron-phonon BCS superconductors: (1) measured isotope effects are small;[14,15] (2) specific heat measurements[16] indicate a small mass enhancement factor; (3) the density of states at the Fermi level is small (when electron doped), and T_c is almost independent of the doping level in the range $0.15 < x < 0.5$. As a feature peculiar to this system, T_c actually increases as the metal-insulator transition at $x_{cr} = 0.06$ is approached, rather than following the common dome shape with doping. Linear response calculations also agree on the small electron-phonon coupling constant[17] which cannot account for the observed T_c. The impressive high transition temperatures and easy tunability of carrier concentrations (and sometimes effective dimensionality) suggest that there is potential to reach higher T_c in this class.[18]

The possible candidates for the pairing mechanism responsible for the observed high T_c are spin and charge fluctuations, which have been discussed by both experimentalists and theorists, but opinions remain controversial. The specific heat measurement on Li_xZrNCl is suggestive of relatively strong coupling superconductivity, based on the observed large gap ratio and specific jump[16] at T_c. The interlayer spacing dependence of T_c reveals the close relation between the pairing interaction and topology of the Fermi surface,[6] implying a spin- and/or charge-induced superconductivity. The magnetic susceptibility measurement of heavily doped $Li_x(THF)_yHfNCl$ indicates low carrier density and negligible mass enhancement factor, in favor of charge fluctuations over spin fluctuations.[19]

A detailed measurement of the doping dependence of specific heat and magnetic susceptibility has been performed on Li_xZrNCl and the data were compared with calculations based on a model Hamiltonian,[20,21] which shows a correlation between T_c and magnetic susceptibility. Some change is occurring that affects both, but a causal relationship has not been established. There have been several band structure calculations for ZrNCl and HfNCl that provide the basis for more specific studies, mostly in the superconducting β structure.[3,22–24]

Recently, Yamanaka *et al.*[2] reported superconductivity in the alkali-metal-intercalated α-TiNCl, with T_c up to 16.5 K. This is the first *MNX* compound found to be superconducting in the α structure. The lack of Fermi surface nesting in α-Li$_x$TiNCl seems to exclude any dramatic magnetic fluctuations, and the lack of evidence for local moment magnetism or temperature-dependent susceptibility makes magnetic fluctuations an unlikely mechanism for pairing. Its low carrier density character is potentially more interesting: weak screening in the background of highly charged ions (such as can be accounted for together[25]), and the strong effect of two-dimensionality on collective charge excitations (the 2D plasmon disperses as $\sqrt{q}$) suggest charge fluctuations as a more likely pairing mechanism.

On the theoretical side, charge-fluctuation-induced superconductivity has been discussed in the Hubbard model,[26,27] the d-p model,[28] and has been applied to study Na$_x$CoO$_2 \cdot y$H$_2$O (Refs. [29] and [30]) and organic molecular superconductors.[31] Spin-fluctuation-mediated pairing has been discussed in relation to cuprate and heavy-fermion superconductivity by numerous authors; see Ref. [32]. The studies have typically considered the strong interaction regime. In the opposite limit, dynamic screening in the homogeneous electron gas has also been studied to assess the possibility of regimes of overscreening that might result in pairing.[33–35] Charge-fluctuation-mediated pairing in real (inhomogeneous) systems but not in the strong interaction limit has been addressed,[8,9] though less often due to the numerous (but interesting) complications that arise.

In one way or another, almost all proposed mechanisms focus on the "susceptibility loop" diagram as providing the generalized boson that results in attraction and hence pairing. This loop, which occurs in the electronic self-energy diagram, has attracted much attention, and approaches from the *ab initio*, density functional viewpoint have gained attention in recent years due to sophisticated codes, improved algorithms, and ever-increasing computational power. Concern in d-electron compounds has extended from the susceptibility (dielectric screening and the magnetic analog) to its effects on the electronic excitation spectrum itself[36,37] and subsequently to the further effects on the susceptibility (mostly focusing on the gap-widening feature).[38,39] The various approximations that have been tried are reflective of the fact that, in the electron-electron interaction, there is no small parameter that allows controlled perturbation-theoretic procedures.

It is evident that a more detailed investigation of the electronic structure and dynamical spin and/or charge susceptibility is needed to study the superconducting mechanism in α-TiNCl. In the present work, we carry out a calculation of spin and charge susceptibilities using a many-body Hamiltonian, based on a realistic band structure calculated by density functional theory and taking into account explicitly on-site (Hubbard U) repulsion, intersite (extended Hubbard) charge repulsion, Hund's rule coupling, and interorbital "pair hopping" processes in a multiband system. These interactions are based on the random phase approximation (RPA), which should be reasonably reliable in systems like these where vertex corrections should not be large. It can be noted that the (exact) density functional expression for the static susceptibility assumes an RPA-like form,[40] with a well-defined prescription of the screened (and correlated) Coulomb interaction in the denominator. Our local orbital basis enables a direct separation of contributions from different orbitals, and among other findings we show that the structure of the susceptibility in the wave vector q is strongly affected by matrix elements.

II. CRYSTAL STRUCTURE

The α structure[2] of the *MNX* class of compounds, often called the FeOCl structure, is shown in Fig. 1, with structural data given in Table I. The α-structure TiNCl belongs to space group *Pmmn* (no. 59), with six atoms per unit cell occupying the following sites: Ti(2b) $(0, \frac{1}{2}, z_{\mathrm{Ti}})$, N(2a) $(\frac{1}{2}, \frac{1}{2}, z_{\mathrm{N}})$, and Cl(2a) $(0, 0, z_{\mathrm{Cl}})$. The generators of *Pmmn* are two simple reflections $x \to -x$ and $y \to -y$, and the nonsymmorphic reflection $z \to -z$, followed by a $(\frac{1}{2}, \frac{1}{2}, 0)$ translation.

The Ti-N net within TiNCl is topologically equivalent to that of a single NaCl layer. There is strong buckling of this Ti-N net perpendicular to the b direction, such that neighboring chains that are directed along a differ in height. These chains are themselves somewhat buckled, all of this leading to the placement of Ti ions ± 0.8 Å from the average height and N ions ± 0.4 Å from the average height. The Ti ions are twofold coordinated by Cl ions lying in the y-z plane; the breaking of square symmetry of the TiN layer by its strong buckling can be regarded as "due to" this positioning of the Cl ions.

Finally, each Ti is sixfold coordinated by four N and two Cl atoms. The two Ti-N bonds have very close lengths of 2.008 and 2.015 Å, respectively, though the N ions lie at different heights in the x and y directions. Very roughly, the Ti ion is in octahedral coordination (see Fig. 5 of Ref. [2]), with approximate axes (1,0,0) (toward two neighboring N ions), and (0,1,1) and (0,1,−1) (each toward one N and one Cl ion),
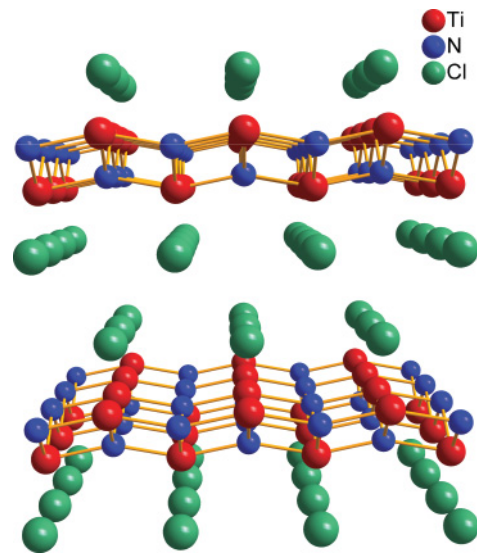

FIG. 1. (Color online) Crystal structure of α-phase TiNCl (*Pmmn*, no. 59). Viewpoint is along the b axis, perpendicular to the buckling of the Ti-N net. The buckled Ti-N layer leaves each Ti coordinated (roughly octahedrally) by four N and two Cl atoms. The Cl coordinates with Ti along the b axis, which accounts for its orthorhombic structure.

TABLE I. Lattice constants (in units of Å) and internal structural parameter z for the three atoms. Experimental values are from Ref. 2. The theoretical values are our optimized values.

	a	b	c	z_{Ti}	z_N	z_{Cl}
Expt.	3.938	3.258	7.800	0.1011	0.0509	0.3322
Theory	3.891	3.200	7.699	0.1011	0.0522	0.3384

and indeed a rough t_{2g}-e_g splitting of the Ti $3d$ states results. The Ti-Ti distance is 3.003 Å, not much larger than that of Ti-N due to the buckled layer structure, so in the tight-binding model we construct in the next section, the hoppings between Ti sites are also important.

The experimental lattice constants and atomic positions, and relaxed structure parameters with respect to total energy, which are used in our calculation, are listed in Table I. The calculations (see below) confirm the expected formal valences. The calculated lattice constants are 1%–1.5% smaller than the experimental values, but this has little effect on the electronic structure. TiNCl is still calculated to be an ionic insulator and its theoretical gap is similar to what is calculated using the experimental lattice parameters.

III. BAND STRUCTURE AND WANNIER FUNCTIONS

A. Methods

The band structure has been computed by the full-potential local orbital minimal basis set method implemented in the FPLO code.[41] The exchange correlation is treated by the generalized gradient approximation GGA96,[42] and the **k** mesh used is $16 \times 16 \times 8$. The effect of spin-orbit coupling is small so calculations were done in the scalar relativistic scheme.

B. Electronic structure

The calculated band structure of pristine TiNCl is shown in Fig. 2 and is generally consistent with that presented by Yamanaka *et al.*[2] plotted along other lines in the zone. It is an
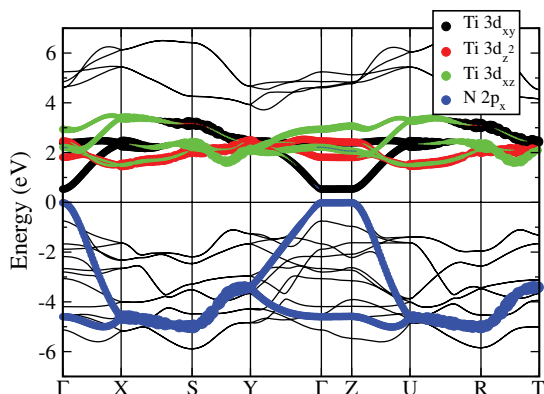

FIG. 2. (Color online) Band structure of TiNCl along the orthorhombic symmetry lines, calculated with the GGA exchange-correlation functional. The thick "fatbands" are the tight-binding representation determined by the Wannier functions labeled in the inset, chosen to represent accurately the bands at and around the Fermi level after doping.
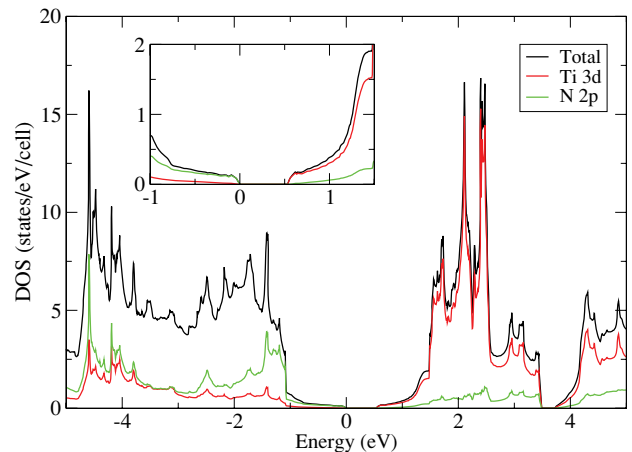

FIG. 3. (Color online) Total and partial densities of states of TiNCl, showing the Ti $3d$–N $2p$ mixing. The inset figure is a blow-up of the region near the Fermi level.

insulator with a calculated energy gap of 0.5 eV. The real band gap may be as large as 1 eV, based on the common observation that the local density approximation and generalized gradient approximation underestimate gaps in insulators. The band structure exhibits clearly a two-dimensional feature, gauged from the general flatness of bands along the Γ-Z direction perpendicular to the layers. The states on either side of the gap are very two dimensional, considering the extreme flatness of those bands along Γ-Z.

The twelve valence bands are made of six N $2p$ and six Cl $3p$ states, and the conduction band is comprised of ten Ti $3d$ states. The $3d$ bands show a "t_{2g}-e_g" crystal field splitting (three states below and two above), which arises in spite of the nonequivalence of the five $3d$ orbitals in this structure. As can be seen in the partial density of states plotted in Fig. 3, there is $3d$ weight in the valence bands and N weight in the conduction bands, reflecting substantial N $2p$–Ti $3d$ hybridization in addition to the ionic character reflected in their formal charges.

Whereas the $3d$ environment appears locally to be pseudocubic, the low site symmetry severely splits the N $2p$ states, with $2p_x$ and $2p_y$ becoming quite distinct. The top valence band has primarily N $2p_x$ character, which extends down to -5 eV. The N p_y and p_z bands have their maximum 1 eV lower, and the Cl $2p$ weight is concentrated at the bottom of the valence bands.

The inset in Fig. 3 shows an enlargement of the total and atom-projected density of states (DOS) around the Fermi energy. The onset at 0.5 eV and the smooth slope to 1.2 eV are characteristic of a two-dimensional band which becomes nonparabolic away from the band edge, and strongly so in the 1.2–1.5 eV region. At 1.5 eV the onset of the second band, with its much heavier mass, is clear. However, the DOS does not have the sharp step at the top of the valence band that is characteristic of a 2D system.

The Ti $3d$ orbitals are lifted in degeneracy entirely by the orthorhombic point group site symmetry, but as mentioned above the conduction bands are separated by a crystal field analogous to cubic t_{2g}-e_g splitting. Checking the band character reveals that, in terms of $3d$ orbitals expressed in

terms of the orthorhombic coordinate axes, d_{xy}, d_{z^2}, d_{xz} have most of the weight in the 0.5–3 eV region, and $d_{yz}, d_{x^2-y^2}$ are in a higher-energy window of 4–6 eV. Thus it is feasible, in a low-energy tight-binding model, to include only Ti d_{xy}, d_{z^2}, d_{xz} and N $2p_x$ states. Plotted on top of the density functional theory (DFT) bands in Fig. 2 is the tight-binding fit using the Wannier functions. The representation of the full t_{2g} complex is excellent, as is that of the top of the upper valence band.

The distance between TiNCl slabs and the weak interlayer coupling allows intercalation of alkali-metal atoms, which act as electron donors. This feature validates the rigid band shift approximation in simulating doping. Doped-in electronic carriers will go into the single lowest conduction band, which is quite two dimensional as mentioned above but is dispersive within the plane. This band has strong Ti $3d_{xy}$ character, similar to the in-plane $4d$ character in ZrNCl. The Fermi surface of electron-doped TiNCl is an oval centered at the Γ point. This point has some relevance for the superconductivity, since with a single Fermi surface there can be no nesting of disconnected Fermi surfaces, such as are proposed[21] to play an important role in many other layered superconductors, such as Fe pnictides, as well as β-structured ZrNCl and HfNCl. The similar characters of TiNCl and ZrNCl, and their similar values of T_c, suggest that possible nesting of Fermi surfaces is not an important feature for pairing in the materials.

C. Wannier functions

Because the susceptibilities we will calculate have a number of local orbital matrix elements equal to the fourth power of the number of orbitals retained, we have calculated selected low-energy Wannier functions (WFs) that will be used to construct our many-body Hamiltonian, using projections of the Bloch states onto the corresponding atomic orbitals. The four atomic orbitals mentioned above allow us to reproduce the bands on either side of the gap: Ti d_{xy}, d_{z^2}, d_{xz} and N p_x. While the Ti "t_{2g}" orbitals are not optimal in diagonalizing the local "octahedral" symmetry, they and their relation to the $2p_x$ orbital are more readily visualized. Since the RPA calculations described below were performed in the electron-doped region where the Fermi level is shifted into the conduction bands, considering only the N p_x WF in the valence band is sufficient to understand the $\mathbf{q}$ dependence. Aside from being farther removed in energy, the remainder of the valence bands form a complex of bands spread uniformly over the zone, contributing little to any $\mathbf{q}$ dependence.

The Ti-N layer is strongly buckled and there are two Ti and two N atoms per unit cell with different z coordinates. The actual tight-binding model contains eight bands and eight WFs, but WFs on symmetry-related ions are symmetry equivalent. Overall, the Wannier orbitals generate a well-represented band structure compared to the DFT bands within the energy window of interest, as shown in Fig. 2.

The hopping amplitudes of the Wannier orbitals are listed in Table II. Hopping integrals smaller than 0.05 eV were not listed because they only marginally alter the band structure and obfuscate interpretation. The on-site energies of the "t_{2g}" orbitals are 2.25 ± 0.08 eV, lying within the largest peak of the DOS. The p_x energy is -3.22 eV, in the middle of the valence bands. Thus there is a 5.5 eV separation of valence and conduction band centers, and a gap of 0.5 eV.

TABLE II. Nearest-, second-, and third-neighbor hopping integrals in units of eV. The hopping vectors are in units of $[a/2, b/2, c]$, and Δz represents the difference between the z coordinates of the two orbitals. This representation is purely two dimensional (no coupling along the c axis).

(μ, ν)	$[0,0,0]$	$[1,0,\Delta z]$	$[0,1,\Delta z]$	$[1,1,\Delta z]$	$[2,0,0]$	$[0,2,0]$
(d_{xy}, d_{xy})	2.33			-0.16	-0.17	-0.18
(d_{xy}, d_{z^2})				-0.08		
(d_{xy}, d_{xz})				0.07		-0.11
(d_{z^2}, d_{z^2})	2.18			-0.05		
(d_{z^2}, d_{xz})				0.19	0.07	
(d_{xz}, d_{xz})	2.25				-0.05	0.13
(d_{xy}, p_x)			-0.33			
(d_{z^2}, p_x)		0.24	0.22			
(d_{xz}, p_x)			0.21			
(p_x, p_x)	-3.22			0.51	0.47	0.14

The dispersion within the pair of valence p_x bands is represented largely by hopping between neighboring p_x WFs (recall that the p_x WF contains some d character, and vice versa), both being about 0.5 eV. Hopping amplitudes to the d orbitals are $t_{pd} \approx 0.2$–0.3 eV. In the conduction bands, the d_{xy} orbital has hopping amplitude $|t| \sim 0.17$ eV to its partner within the cell as well as to its replicas in neighboring cells in both directions. The hopping to the p_x orbital (0.33 eV) is twice as large, and apparently is the dominant contributor to the 3.5 eV bandwidth. Due to the relative orientations, hopping to the other d WFs is no more than half as large as the d_{xy}-d_{xy} one. The other two d WFs form rather narrow bands, reflected by smaller hopping amplitudes; note that both have hopping to the p_x orbital of 0.21–0.24 eV.

IV. MANY-BODY HAMILTONIAN AND RANDOM PHASE APPROXIMATION

The random phase approximation applies an interaction to the noninteracting Hamiltonian

$$H_0 = \sum_{\mathbf{k}, ab} H_{ab}^{\mathbf{k}} c_{\mathbf{k},a}^{\dagger} c_{\mathbf{k},b}, \qquad (1)$$

where a and b are composite orbital and spin indices of the basis Wannier orbitals. The interaction Hamiltonian, in general, is in the following symmetric form:

$$H_1 = \frac{1}{2} \sum_i \sum_{abcd} U_{abcd} c_{ia}^{\dagger} c_{ib} c_{ic}^{\dagger} c_{id} + \sum_{\langle i,j \rangle} \sum_{abcd} V_{abcd} c_{ia}^{\dagger} c_{ib} c_{jc}^{\dagger} c_{jd}, \qquad (2)$$

where U and V represent on-site and intersite (only nearest neighbors) interactions, respectively. Equation (2) can be Fourier transformed into

$$H_1 = \frac{1}{2N} \sum_{\mathbf{kpq}} \sum_{abcd} F_{abcd}(\mathbf{q}) c_{\mathbf{k},a}^{\dagger} c_{\mathbf{k}+\mathbf{q},b} c_{\mathbf{p}+\mathbf{q},c}^{\dagger} c_{\mathbf{p}d}, \qquad (3)$$

in which $F_{abcd}(\mathbf{q}) = U_{abcd} + \gamma(\mathbf{q}) V_{abcd}$ is the interaction kernel matrix. In the second term, $\gamma(\mathbf{q}) = \sum_l e^{i\mathbf{q} \cdot \mathbf{R}_l}$ (l running over the nearest-neighbor pairs of sites) is the structure

factor, which brings in **q** dependence into $F_{abcd}(\mathbf{q})$. The bare susceptibility is calculated as

$$\chi^0_{abcd}(\mathbf{q},\omega) = \sum_{\mathbf{k}} G_{ad}(\mathbf{k},\omega) G_{cb}(\mathbf{k}+\mathbf{q},\omega), \qquad (4)$$

where $G_{ab}(\mathbf{k},\omega)$ is the noninteracting Green's function

$$G_{ab}(\mathbf{k},\omega) = \sum_{n} \frac{\langle a| n\mathbf{k}\rangle \langle n\mathbf{k} |b\rangle}{\omega + \mu - \varepsilon_{n\mathbf{k}}}, \qquad (5)$$

and the summation is taken over all bands. Applying the RPA, which sums up the higher-order diagrams in the geometric series, we have the full susceptibility presented in a matrix equation

$$\chi(\mathbf{q},\omega) = [I + \chi^0(\mathbf{q},\omega)\mathrm{Re}F(\mathbf{q})]^{-1}\chi^0(\mathbf{q},\omega), \qquad (6)$$

where a matrix χ is formed from χ_{abcd} by contracting the first pair of indices and the last pair of indices.

So far we have derived a very general formula for an arbitrary interaction Hamiltonian. To study our case, next consider a more specific model in the form of an extended Hubbard Hamiltonian, following Kuroki *et al.*'s model,[43] but add an extra intersite interaction term:

$$\begin{aligned} H_1 = \sum_{i} \Bigg[& U \sum_{a} n_{ia\uparrow}n_{ia\downarrow} + U' \sum_{a\neq b}\sum_{\sigma,\sigma'} n_{ia\sigma}n_{ib\sigma'} \\ & - J \sum_{a\neq b} S_{ia}\cdot S_{ib} + J' \sum_{a\neq b} c^\dagger_{ia\uparrow}c^\dagger_{ia\downarrow}c_{ib\downarrow}c_{ib\uparrow} \Bigg] \\ & + \sum_{\langle i,j\rangle}\sum_{a,b} V_{ab}n_{ia}n_{jb}, \end{aligned} \qquad (7)$$

in which a,b are orbital indices, i,j are site indices of the lattice, and σ is the spin index. U is the intraorbital Coulomb repulsion, U' is the interorbital Coulomb interaction, $t^{\mu\nu}_{ij}$ is the hopping between Wannier orbitals, V_{ab} is the intersite Coulomb interaction between orbitals a and b, J is the Hund's rule coupling, and J' refers to pair hopping between orbitals. From this Hamiltonian, the susceptibility is calculated by

$$\begin{aligned} \chi^S(\omega,\mathbf{q}) &= \frac{\chi^0(\omega,\mathbf{q})}{I - S(\mathbf{q})\chi^0(\omega,\mathbf{q})}, \\ \chi^C(\omega,\mathbf{q}) &= \frac{\chi^0(\omega,\mathbf{q})}{I + C(\mathbf{q})\chi^0(\omega,\mathbf{q})}. \end{aligned} \qquad (8)$$

The interaction matrices $S(\mathbf{q})$ and $C(\mathbf{q})$ take the form

$$S_{abcd} = \begin{cases} U, & a = b = c = d \\ U', & a = c \neq b = d \\ J, & a = b \neq c = d \\ J', & a = d \neq b = c \end{cases}, \qquad (9)$$

$$C_{abcd} = \begin{cases} U + 2V_{ac}\,\mathrm{Re}\,\gamma(\mathbf{q}), & a = b = c = d \\ -U' + J, & a = c \neq b = d \\ 2U' - J + 2V_{ac}\,\mathrm{Re}\,\gamma(\mathbf{q}), & a = b \neq c = d \\ J', & a = d \neq b = c \end{cases},$$

where U, U', J, and J' terms appear only if all indices are orbitals on the same site. Finally, we can also calculate the

macroscopic susceptibilities by performing a summation over the orbital indices:

$$\chi^{\mathrm{mac}}(\mathbf{q},\omega) = \sum_{ijkl} S_{ij}\chi_{ijkl}(\mathbf{q},\omega)S_{kl}, \qquad (10)$$

in which S_{ij} is the overlap matrix, and in our case it has the form of a delta function δ_{ij}.

V. SPIN AND CHARGE SUSCEPTIBILITY

With our model just constructed, we calculate the spin and charge susceptibilities. The model is a multiband extended Hubbard model on a 2D rectangular lattice with four sites (two Ti and two N) per unit cell. For the on-site interaction terms, we use $U_{dd} = U'_{dd} = 1.5$ eV, $U_{pp} = 1.0$ eV, and $J = J' = 0.2$ eV. These values are somewhat smaller than might be used in a traditional Hubbard model calculation; this is partly to compensate for the fact that the RPA has a tendency to overestimate the strength of the interaction due to the lack of the self-energy correction.[43] Moreover, we are using WFs rather than atomic orbitals, for which the extension onto neighboring sites will suppress the intra-atomic interactions U and J.

For intersite interactions, we assume V_{ac} to be spin and orbital independent, and that it only depends on the distance between the two sites. Taking into account the Ti-N and Ti-Ti distances mentioned above, we use $V_{\mathrm{Ti-N}} = 0.5$ eV (nearest neighbor), $V_{\mathrm{Ti-Ti}} = 0.3$ eV (second-nearest neighbor). Since the Wannier functions have contributions from neighboring sites, it is reasonable to set the intersite Coulomb repulsion V slightly larger than traditionally used for atomic orbitals. The calculation is done at $T = 0.02$ eV (220 K) and $\omega = 0$, with a **k** mesh of $40 \times 40 \times 4$ and **q** mesh of $20 \times 20 \times 2$. The occupation is set at 4.3, simulating $x = 0.15$ electron doping in $A_{0.15}$ TiNCl (since there are two formula units per unit cell) by raising the Fermi level into the lowest conduction band.

Figure 4 shows the magnitude of the imaginary part of Green's function, which provides a view of the Fermi surface. With a simple, nearly circular Fermi surface like this, the bare susceptibility is expected[44] to be isotropic out to $q = 2k_F$, with a relatively constant plateau behavior inside $2k_F$ radius. The intersite Coulomb
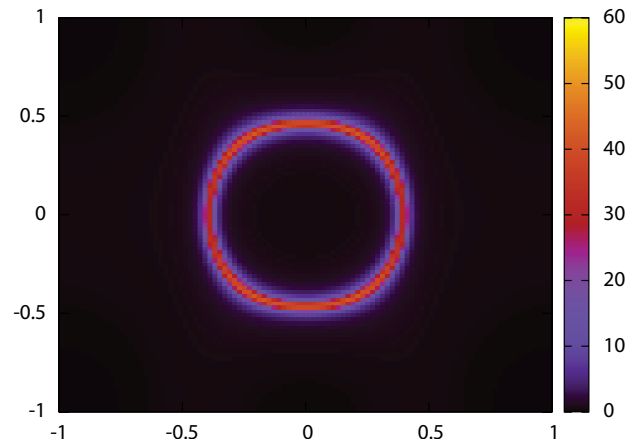

FIG. 4. (Color online) The spectral function $-\mathrm{Im}G(\mathbf{k},\omega = 0)$ in the k_x-k_y plane, showing the oval (nearly circular) Fermi surface for $x = 0.15$ electron doping.

interaction can give rise to charge fluctuation, creating collective electron motion and possible charge ordering. Competition between on-site and intersite interaction of d electrons can lead in principle to a frustration of both spin and charge ordering. The hybridization between d and p orbitals opens another channel, that of a charge transfer instability. One of the interesting questions is whether some combination of these processes can create excitations that can pair up electrons, analogous to the behavior found in a d-p model in the limit of infinite U and nearest-neighbor hybridization.[28]

In Fig. 5 some representative spin susceptibilities in the orbital representation are plotted on the two-dimensional basal plane ($q_z = 0$) in the Brillouin zone (BZ). Since our hopping integrals have units of eV, the susceptibilities are in units of

1/eV. To clarify, we denote the orbitals by numbers in the order (1)Ti$_1$ d_{xy}, (2)Ti$_2$ d_{xy}, (3)Ti$_1$ d_{z^2}, (4)Ti$_2$ d_{z^2}, (5)Ti$_1$ d_{xz}, (6)Ti$_2$ d_{xz}, (7)N$_1$ p_x, (8)N$_2$ p_x. The largest spin susceptibility is found for χ^S_{1111} (intersite, $xy \leftrightarrow xy$) which has approximate fourfold symmetry for magnetic fluctuations of the same orbital d_{xy} on Ti sites. The anisotropic behavior of χ^S_{1133} (on site, $xy \leftrightarrow z^2$) comes from the orthorhombic symmetry of the lattice, i.e., $a \neq b$, which brings in anisotropic $\mathbf{q}$ dependence, in this case strongly so. The spin fluctuations between d and p orbitals, χ^S_{1177}, have a sizable overall magnitude, comparable to d-d fluctuation, but small variation with $\mathbf{q}$, because four neighboring N atoms have almost the same distance to Ti. Due to the lack of Fermi surface nesting, there is no divergent behavior in the spin susceptibility, presenting different physics from that for β-HfNCl, which has two circular Fermi surfaces located at two high-symmetry (K) points in the BZ that can provide near-perfect nesting.

Representative charge susceptibilities are shown in Fig. 6. Often they have similiarities to the spin susceptibilities, with comparable but somewhat smaller magnitudes. It is known that in an extended Hubbard model on a square lattice, at zero frequency, χ^S and χ^C have similar $\mathbf{q}$ dependence and only vary in magnitude.[45] Without the long-range Coulomb interaction, charge fluctuation will always be smaller than spin fluctuation because of the different signs in the RPA formula. The difference between χ^S and χ^C will become more apparent at nonzero ω. The $\mathbf{q}$ dependence of χ^C is similar to that of χ^S but shows somewhat more structure in χ^C_{1111}. Note
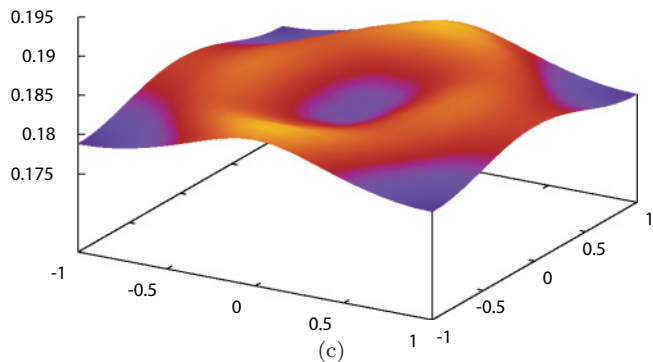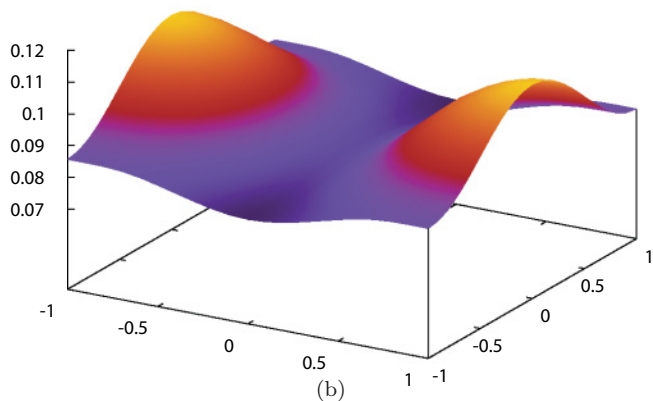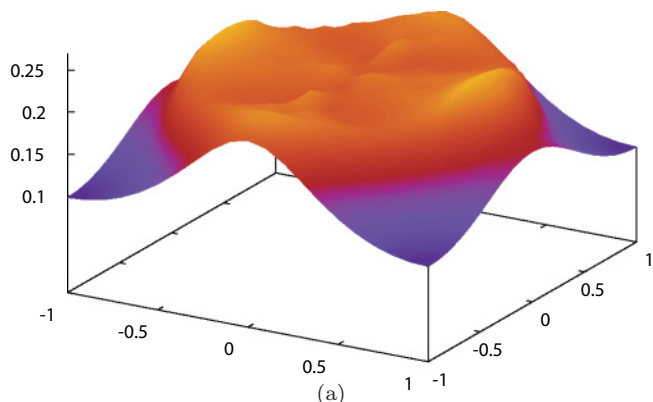

(a)

(b)

(c)

FIG. 5. (Color online) Representative orbital spin susceptibilities (units: 1/eV). In the basal plane, the axis on the left (longer in perspective) is q_x axis (in units of π/a), and the one on the right (shorter) is q_y axis (in units of π/b). (a) χ^S_{1111}, (b) χ^S_{1133}, and (c) χ^S_{1177}. Note that the maximum in χ^S_{1133} is located at $(\pi/a,0,0)$ and not at $2k_F$. Note the different vertical scales on the panels.

(a)

(b)

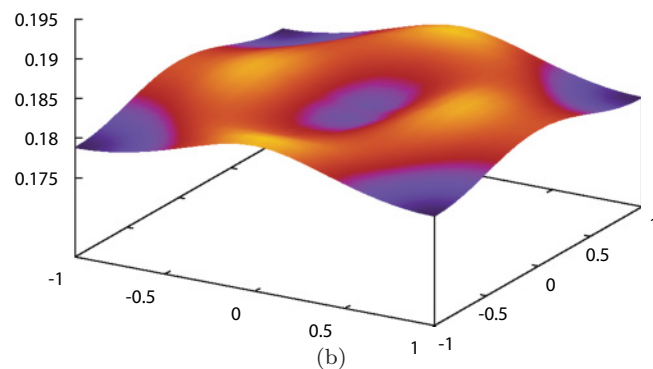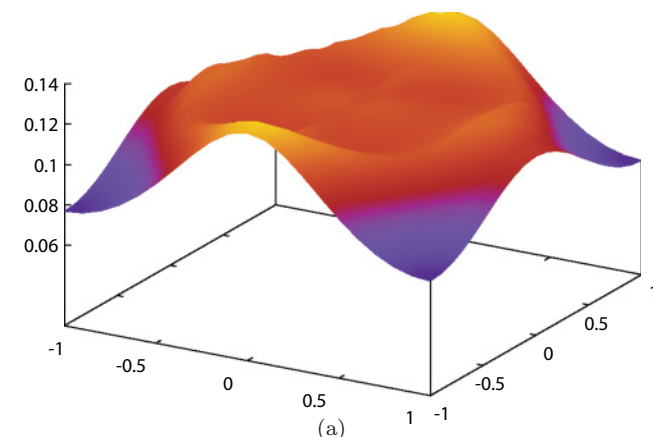FIG. 6. (Color online) Representative charge susceptibilities in the full Brillouin zone. (a) χ^C_{1111} and (b) χ^C_{1177}. The latter quantity is hardly distinguishable from its spin counterpart. Note the different vertical scales on the panels.
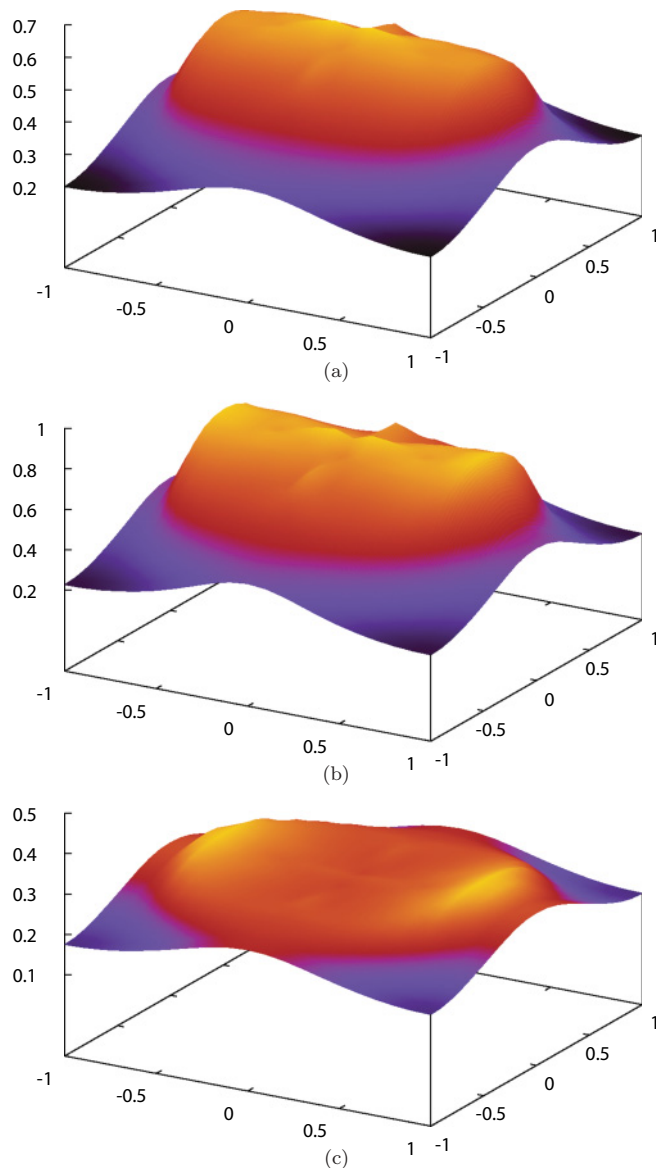
FIG. 7. (Color online) Macroscopic susceptibility: (a) bare; (b) spin; (c) charge. Note the strong deviation from square symmetry.

that the magnitude of χ_{1111}^{C} is only half that of χ_{1111}^{S}. The spin and charge fluctuations within the N p channel are very small since the p orbitals are fully occupied so fluctuations happen only as a second-order effect. However, the presence of the N p band very close to the lowest d conduction band opens an additional channel for fluctuations between them [χ_{1177}^{S}, Fig. 5(c), and χ_{1177}^{C}, Fig. 6(b)].

To close the comparison, we show the macroscopic susceptibilities in Figure 7. The imprint of $2k_F$ is evident. Beyond $2k_F$, the susceptibilities decrease slightly and with (nearly) square symmetry. Inside $2k_F$, the variation is greater and displays the rectangular symmetry of the lattice. The overall spin enhancement of the macroscopic susceptibility [$\chi^S(q)/\chi^0(q)$] near $\mathbf{q} = \mathbf{0}$ is about 1.4. For the model with the realistic parameters considered here, our test calculations show that χ^S will approach divergent behavior when $U \sim$ 4 eV. Since TiNCl has wide $3d$ bands, it is unphysical to use U anywhere near 4 eV (we are using 1.5 eV),

so strong spin fluctuation is unlikely to occur in this material. The macroscopic charge susceptibility has smaller magnitude and $\mathbf{q}$ dependence, but will show divergent behavior when intersite interaction V is much larger than U, but that regime is unrealistic for the case studied here. Overall, both spin and charge susceptibilities show moderate enhancements compared to the bare susceptibility, without any approach to an instability toward spin or charge ordering.

VI. SUMMARY

In this work we have constructed a many-body extended Hubbard model based on a realistic band structure obtained from density functional theory calculations. The random phase approximation was applied to obtain the spin and charge susceptibilities. In a system like α-TiNCl, where the crucial ingredients of high-temperature superconductivity, such as strong electron-phonon coupling and good Fermi surface nesting, seem to be missing, spin and charge fluctuations are the remaining candidates. The Wannier local orbital basis both is a physical basis, building in bonding effects, and promotes the study of orbital-dependent contributions to the susceptibilities. These orbital-dependent matrix element effects are very strong, with the character of the electron and hole bands determining the strength and character of the q dependence.

Our calculations show that the spin and charge enhancements of susceptibilities, both intraband and interband, are modest in magnitude due to moderate correlations. However, spin and charge fluctuations can produce substantial values possibly capable of encouraging electrons to pair. One of the most detailed studies of such effects is that of Monthoux and Lonzarich,[32] who note a "surprisingly rich behavior even for our chosen simple tight-binding band." Generalizing to the multiband system with intersite interaction that we have treated seems futile; seemingly innocuous changes in interaction strengths or doping level, or perhaps even the underlying atomic structure, may have appreciable effect on the resulting phenomena, so realistic models must become increasingly more material specific to be useful in understanding superconducting tendencies.

Although spin fluctuations, from our calculations, are present to some degree in α-TiNCl, it is worth repeating that the physics seems very different from the β-structure counterparts (no Fermi surface nesting) even though both are nonmagnetic and seem similar in many ways. This class of transition-metal nitrides is apparently quite distinct from the recently discovered Fe pnictides, where magnetism is a dominating feature in the parent compounds. As the nonmagnetic nature of TiNCl and other MNX materials indicates, as well as seen from the results from our RPA calculation, charge fluctuations may play the important role in superconductivity in these systems, rather than spin fluctuations. Simply put, we do not have a clear understanding of how superconductivity arises from the fluctuations, as with all other high-T_c families.

ACKNOWLEDGMENTS

*Present address: Department of Physics and Astronomy, Rutgers University, Piscataway, NJ 08854.

[1] X. Chen, T. Koiwasaki, and S. Yamanaka, J. Phys. Condens. Matter **14**, 11209 (2002).

[2] S. Yamanaka, T. Yasunaga, K. Yamaguchi, and M. Tagawa, J. Mater. Chem. **19**, 2573 (2009).

[3] R. Weht, A. Filippetti, and W. E. Pickett, Europhys. Lett. **48**, 320 (1999).

[4] Y. Taguchi, A. Kitora, and Y. Iwasa, Phys. Rev. Lett. **97**, 107001 (2006).

[5] S. Yamanaka, K. Hotehama, and H. Kawaji, Nature (London) **392**, 580 (1998).

[6] T. Takano, T. Kishiume, Y. Taguchi, and Y. Iwasa, Phys. Rev. Lett. **100**, 247005 (2008).

[7] S. Yamanaka, L. Zhu, X. Chen, and H. Tou, Physica B **328**, 6 (2003).

[8] A. Bill, H. Morawitz, and V. Z. Kresin, Phys. Rev. B **66**, 100501(R) (2002).

[9] A. Bill, H. Morawitz, and V. Z. Kresin, Phys. Rev. B **68**, 144519 (2003).

[10] J. K. Jain and P. B. Allen, Phys. Rev. B **32**, 997 (1985).

[11] T. Takasaki, T. Ekino, H. Fujii, and S. Yamanaka, J. Phys. Soc. Jpn. **74**, 2586 (2005).

[12] T. Ekino, T. Takasaki, H. Fujii, and S. Yamanaka, Physica C **388-389**, 573 (2003).

[13] T. Ekinoa, T. Takasaki, T. Muranaka, H. Fujii, J. Akimitsu, and S. Yamanaka, Physica B **328**, 23 (2003).

[14] H. Tou, Y. Maniwa, and S. Yamanaka, Phys. Rev. B **67**, 100509(R) (2003).

[15] Y. Taguchi, T. Kawabata, T. Takano, A. Kitora, K. Kato, M. Takata, and Y. Iwasa, Phys. Rev. B **76**, 064508 (2007).

[16] Y. Taguchi, M. Hisakabe, and Y. Iwasa, Phys. Rev. Lett. **94**, 217002 (2005).

[17] R. Heid and K.-P. Bohnen, Phys. Rev. B **72**, 134527 (2005).

[18] S. Yamanaka, Annu. Rev. Mater. Sci. **30**, 53 (2000).

[19] H. Tou, Y. Maniwa, T. Koiwasaki, and S. Yamanaka, Phys. Rev. Lett. **86**, 5775 (2001).

[20] Y. Kasahara, T. Kishiume, T. Takano, K. Kobayashi, E. Matsuoka, H. Onodera, K. Kuroki, Y. Taguchi, and Y. Iwasa, Phys. Rev. Lett. **103**, 077004 (2009).

[21] K. Kuroki, Sci. Tech. Adv. Mater. **9**, 044202 (2008).

[22] I. Hase and Y. Nishihara, Phys. Rev. B **60**, 1573 (1999).

[23] I. Hase and Y. Nishihara, Physica B **281-282**, 788 (2000).

[24] H. Sugimoto and T. Oguchi, J. Phys. Soc. Jpn. **73**, 2771 (2004).

[25] P. B. Allen, M. L. Cohen, and D. R. Penn, Phys. Rev. B **38**, 2513 (1988).

[26] F. Bucci, C. Castellani, C. Di Castro, and M. Grilli, Phys. Rev. B **52**, 6880 (1995).

[27] Y. M. Vilk, Liang Chen, and A. M. S. Tremblay, Phys. Rev. B **49**, 13267 (1994).

[28] M. Azami, A. Kobayashi, T. Matsuura, and Y. Kuroda, Physica C **259**, 227 (1996).

[29] M. Mochizuki, Y. Yanase, and M. Ogata, Phys. Rev. Lett. **94**, 147005 (2005).

[30] Y. Tanaka, Y. Yanase, and M. Ogata, Physica B **359**, 591 (2005).

[31] J. Merino and R. H. McKenzie, Phys. Rev. Lett. **87**, 237002 (2001).

[32] P. Monthoux and G. G. Lonzarich, Phys. Rev. B **71**, 054504 (2005), and references therein.

[33] H. Rietschel and L. J. Sham, Phys. Rev. B **28**, 5100 (1983).

[34] M. Grabowski and L. J. Sham, Phys. Rev. B **29**, 6132 (1984).

[35] Y. Takada, Phys. Rev. B **39**, 11575 (1989).

[36] S. V. Faleev, M. van Schilfgaarde, and T. Kotani, Phys. Rev. Lett. **93**, 126406 (2004).

[37] C. Rödl, F. Fuchs, J. Furthmüller, and F. Bechstedt, Phys. Rev. B **79**, 235114 (2009).

[38] M. Gatti, F. Bruneval, V. Olevano, and L. Reining, Phys. Rev. Lett. **99**, 266402 (2007).

[39] H. Jiang, R. I. Gomez-Abal, P. Rinke, and M. Scheffler, Phys. Rev. B **82**, 045108 (2010).

[40] J. F. Janak, Phys. Rev. B **16**, 255 (1977).

[41] K. Koepernik and H. Eschrig, Phys. Rev. B **59**, 1743 (1999).

[42] J. P. Perdew, K. Burke, and M. Ernzerhof, Phys. Rev. Lett. **77**, 3865 (1996).

[43] K. Kuroki, H. Usui, S. Onari, R. Arita, and H. Aoki, Phys. Rev. B **79**, 224511 (2009).

[44] W. E. Pickett, J. Supercond. Novel Magn. **19**, 291 (2006).

[45] K.-K. Voo, W. C. Wu, J.-X. Li, and T. K. Lee, Phys. Rev. B **61**, 9095 (2000).